Supporting Information

A Laser-Activated Biocompatible Theranostic Nanoagent for Targeted Multimodal Imaging and Photothermal Therapy

Liming Deng,[†] Xiaojun Cai, [‡] Danli Sheng,[†] Yang Yang,[†] Eric M. Strohm,[§] Zhigang Wang,[†] Haitao Ran,[†] Dong Wang,[⊥] Yuanyi Zheng,[†] Pan Li,[†] Tingting Shang,[†] Yi Ling,[†] Fengjuan Wang,[†] Yang Sun[*,†]

[†]Institute of Ultrasound Imaging & Department of Ultrasound, The Second Affiliated Hospital of Chongqing Medical University; Chongqing Key Laboratory of Ultrasound Molecular Imaging, 400010 Chongqing P. R. China;

[‡]State Key Laboratory of High Performance Ceramics and Superfine Microstructure, Shanghai Institute of Ceramics, Chinese Academy of Sciences 200050, Shanghai, P. R. China;

[§]Department of Mechanical and Industrial Engineering, University of Toronto, Toronto M5S 2E8, Canada;

[⊥]Department of Ultrasound, The First Affiliated Hospital of Chongqing Medical University, 400016 Chongqing P. R. China.

[*]Corresponding to Yang Sun:

E-mail: 300006@hospital.cqmu.edu.cn.

1. Calculation of the photothermal conversion efficiency is as follows:

The HER-DIR-SPIO-PLGA/PFP aqueous solutions (1 mg/mL) in Eppendorf tubes were irradiated with a laser power density of 2 W/cm^2 for 10 min, and then the laser was turned off. The laser spot was adjusted to cover the entire surface of the sample. Pure water was used as a negative control. Real-time thermal imaging of samples was recorded using an IR thermal camera and quantified by FLIR Examiner software.

Following Roper's report [1], the total energy balance for the system can be expressed by Eq. 1:

$$\sum_i m_i \, c_{p,i} \frac{dT}{dt} = Q_{NP} + Q_{Dis} - Q_{Surr} \tag{1}$$

where m and c_p are the mass and heat capacity of water, respectively, T is the solution temperature, Q_{NP} is the energy from the NPs, Q_{Dis} is the baseline energy inputted by the sample cell, and Q_{Surr} is heat conduction away from the system surface by air. The laser-induced source term, Q_{NP}, represents heat dissipated by electron-phonon relaxation of the plasmons on the HER-DIR-SPIO-PLGA/PFP NPs surface under the irradiation of 808 nm laser:

$$Q_{NP} = I(1 - 10^{-A_{808}})\eta \tag{2}$$

Where I is incident laser power, η is the conversion efficiency from incident laser energy to thermal energy, and A_{808} is the absorbance of the HER-DIR-SPIO-PLGA/PFP NPs at wavelength of 808 nm. The source term, Q_{Dis}, expresses heat dissipated from light absorbed by the quartz sample cell itself, and it was measured independently to be 25.1 mW. Furthermore, Q_{Surr} is linear with temperature for the outgoing thermal energy, as given by Eq. 3:

$$Q_{surr} = hS(T - T_{Surr}) \tag{3}$$

where h is heat transfer coefficient, S is the surface area of the container, and T_{Surr} is the ambient temperature of the surroundings.

Once the laser power is defined, the heat input ($Q_{NP} + Q_{Dis}$) will be finite. Since the heat output (Q_{Surr}) is increased along with the increase of the temperature according to the Eq. 3, the system temperature will rise to a maximum when the heat input is equal to heat output:

$$Q_{NP} + Q_{Dis} = Q_{Surr-Max} = hS(T_{Max} - T_{Surr}) \tag{4}$$

where the $Q_{Surr-Max}$ is heat conduction away from the system surface by air when the sample cell reaches the equilibrium temperature, and T_{Max} is the equilibrium temperature. The 808 nm laser heat conversion efficiency (η) can be determined by substituting Eq.2 for Q_{NP} into Eq. 4 and rearranging to get

$$\eta = \frac{hS(T_{Max} - T_{Surr}) - Q_{Dis}}{I(1 - 10^{-A_{808}})} \tag{5}$$

where Q_{Dis} was measured independently to be 25.1 mW, the ($T_{Max} - T_{Surr}$) was 12.2 °C according to Figure S3a, I is 2 W/cm^2, $A808$ is the absorbance (2.054) of HER-DIR-SPIO-PLGA/PFP at 808 nm. Thus, only the hS remains unknown for calculating η.

In order to get the hS, a dimensionless driving force temperature, θ is introduced using the maximum system temperature, T_{Max}

$$\theta = \frac{T - T_{Surr}}{T_{Max} - T_{Surr}} \tag{6}$$

and a sample system time constant τ_s

$$\tau_s = \frac{\sum_i m_i c_{p,i}}{hS} \tag{7}$$

which is substituted into Eq. 1 and rearranged to yield

$$\frac{d\theta}{dt} = \frac{1}{\tau_s}\left[\frac{Q_{NP} + Q_{Dis}}{hS(T_{Max} - T_{Surr})} - \theta\right] \tag{8}$$

At the cooling stage of the aqueous dispersion of the HER-DIR-SPIO-PLGA/PFP, the light source was shut off, the $Q_{NP} + Q_{Dis} = 0$, reducing the Eq. 9

$$dt = -\tau_s \frac{d\theta}{\theta} \tag{9}$$

and integrating, giving the expression

$$t = -\tau_s \ln\theta \tag{10}$$

Therefore, time constant for heat transfer from the system is determined to be $\tau_s = 215\ s$ by applying the linear time data from the cooling period (after 380 s) vs negative natural logarithm of driving force temperature (Figure S3b). In addition, the m_D is 0.3 g and the C_D is 4.2 J/g. Thus, according to Eq. 7, the hS is deduced to be 5.86 mW/°C. Substituting 5.86 mW/°C of the hS into Eq. 5, the 808 nm laser heat conversion efficiency (η) of HER-DIR-SPIO-PLGA/PFP can be calculated to be 5.9%.

2. Supporting Figures

a

	Mean (mV)	Area (%)	St Dev (mV)
Zeta Potential (mV): -1.78	Peak 1: -1.78	100.0	3.57
Zeta Deviation (mV): 3.57	Peak 2: 0.00	0.0	0.00
Conductivity (mS/cm): 0.562	Peak 3: 0.00	0.0	0.00
Result quality : Good			
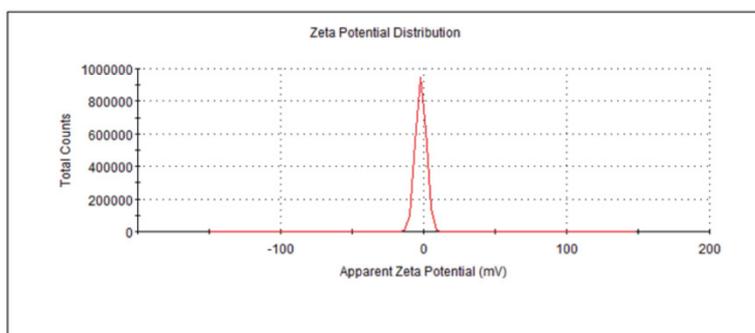
b

	Mean (mV)	Area (%)	St Dev (mV)
Zeta Potential (mV): -2.61	Peak 1: -2.61	100.0	3.53
Zeta Deviation (mV): 3.53	Peak 2: 0.00	0.0	0.00
Conductivity (mS/cm): 0.249	Peak 3: 0.00	0.0	0.00
Result quality : Good			
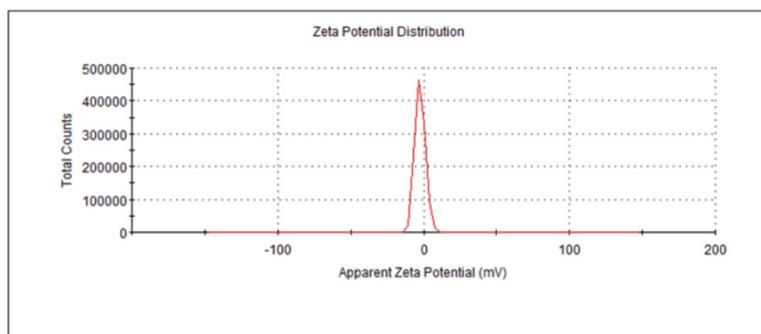
Figure S1. Zeta potential of a) HER-DIR-SPIO-PLGA/PFP and b) DIR-SPIO-PLGA/PFP

nanoparticles.
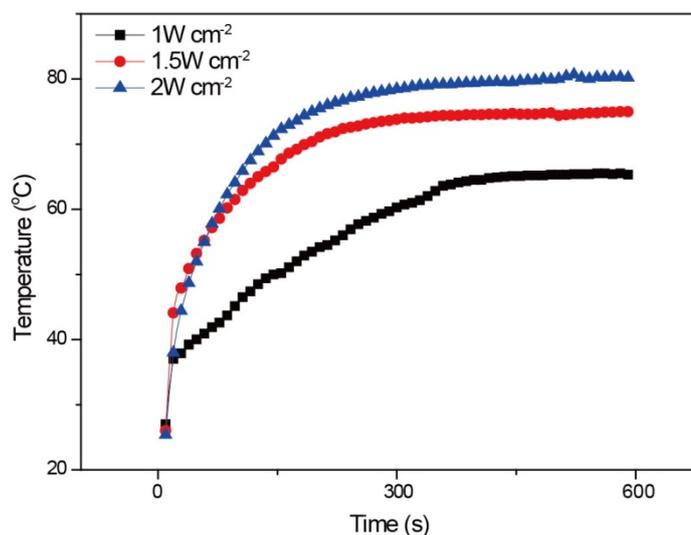
Figure S2. Photothermal curves of 11.25 mg mL^{-1} DIR-SPIO-PLGA/PFP nanoparticles irradiated with different power densities (1 W cm^{-2}, 1.5 W cm^{-2}, 2 W cm^{-2}) for 10 min.
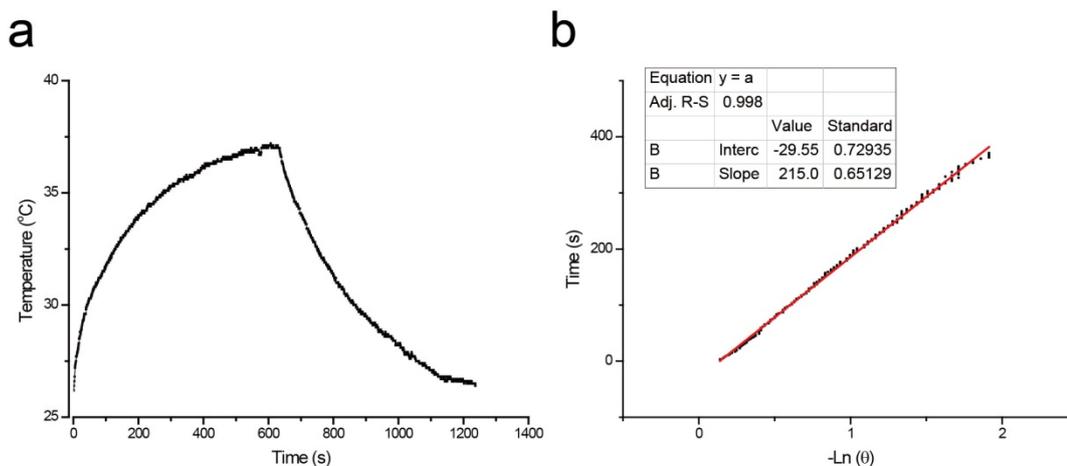
Figure S3. a) Temperature elevation of aqueous solutions of HER-DIR-SPIO-PLGA/PFP exposed to the NIR laser (808 nm, 2 W cm^{-2}). Irradiation was continued for 10 min, and then the laser was turned off. b) Time constant for heat transfer from the system is determined to be $\tau s = 215$ s by applying the linear time data from the cooling period (after 380 s) versus negative natural logarithm of driving force temperature, which is obtained from the cooling stage of figure S3a.
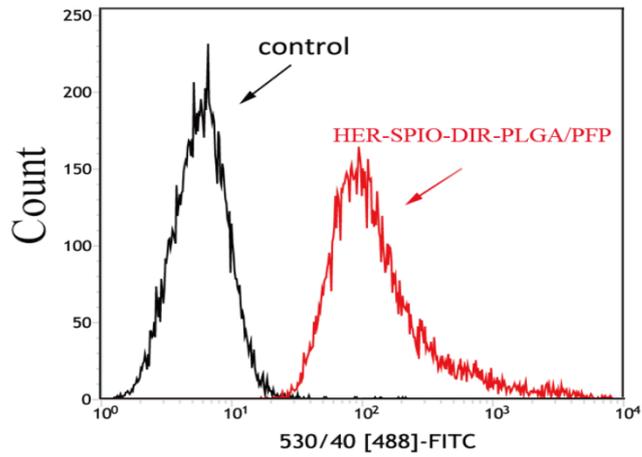
Figure S4. Conjugation rate of Herceptin with targeted nanoparticles and non-targeted nanoparticles analyzed by flow cytometry.
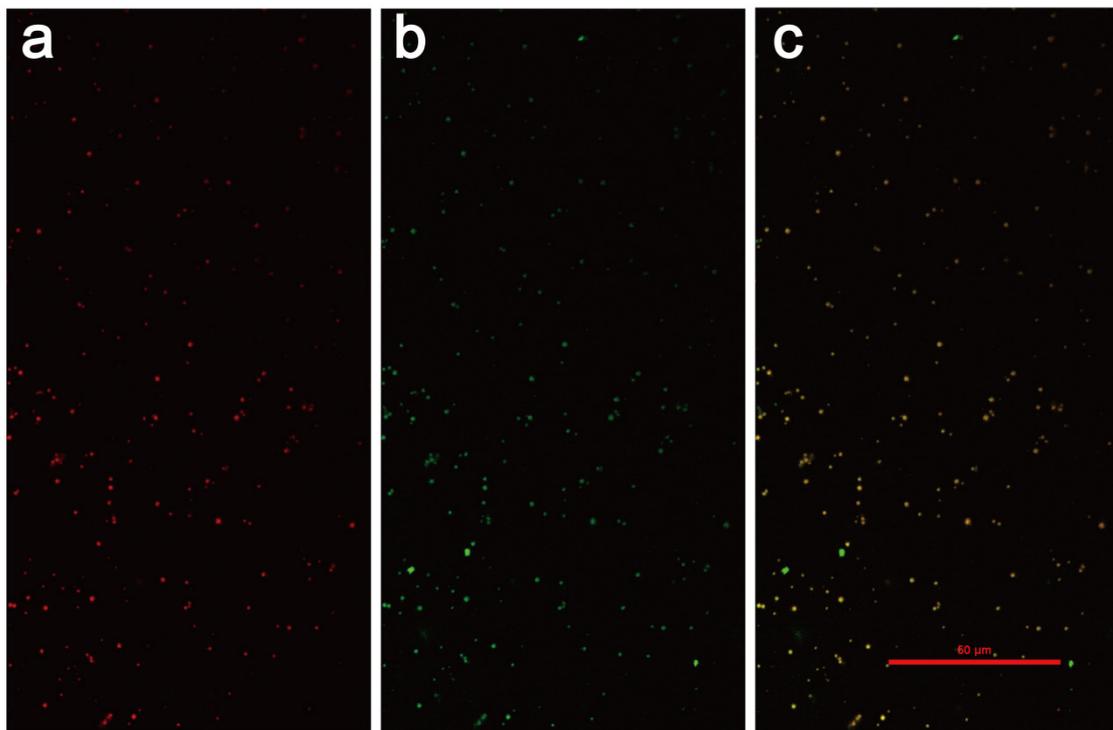
Figure S5. Confocal laser scanning microscopy images of HER2 targeted nanoparticles incubated with FITC-labeled rabbit anti-human antibody for 2 h. a) DiI-labeled nanoparticles, b) FITC-labeled rabbit anti-human antibody, c) merged image.
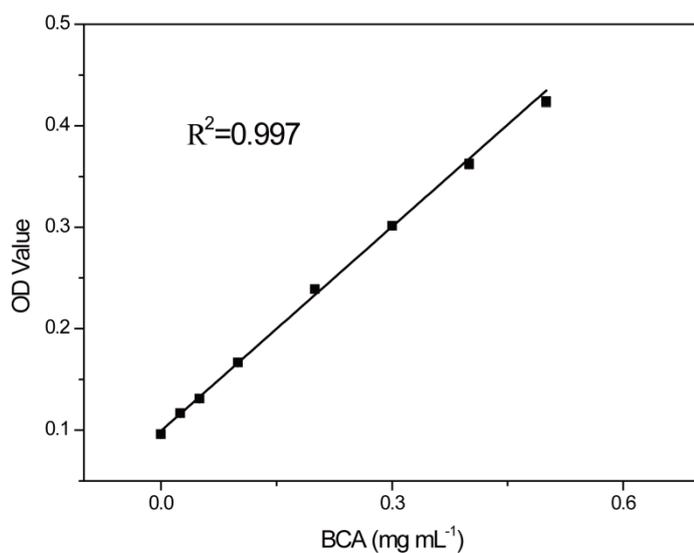
Figure S6. The concentration-absorbance standard curve of bicinchoninic acid (BCA) protein.
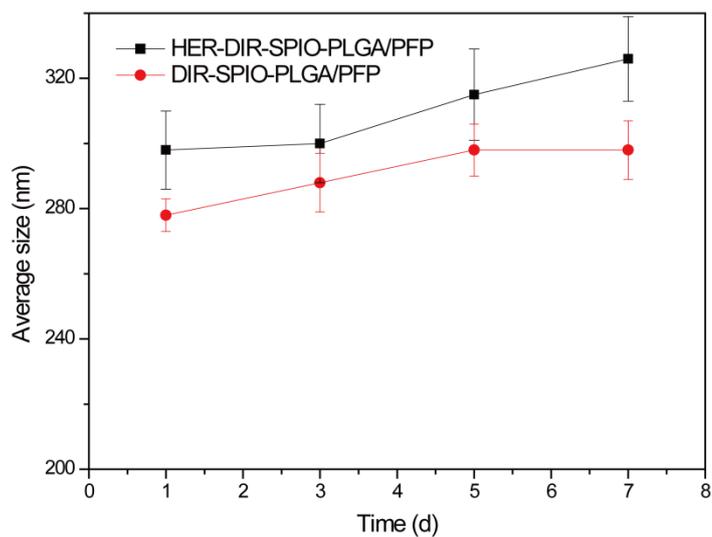
Figure S7. Average size distribution of targeted nanoparticles and non-targeted nanoparticles over 7 days.
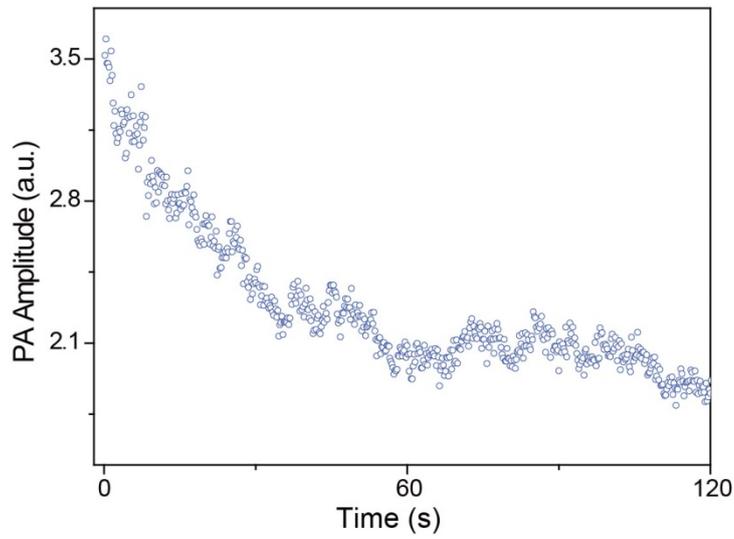
Figure S8. The photoacoustic signal amplitude of the DIR-SPIO-PLGA/PFP during pulsed laser irradiation over a time period of 120 seconds.
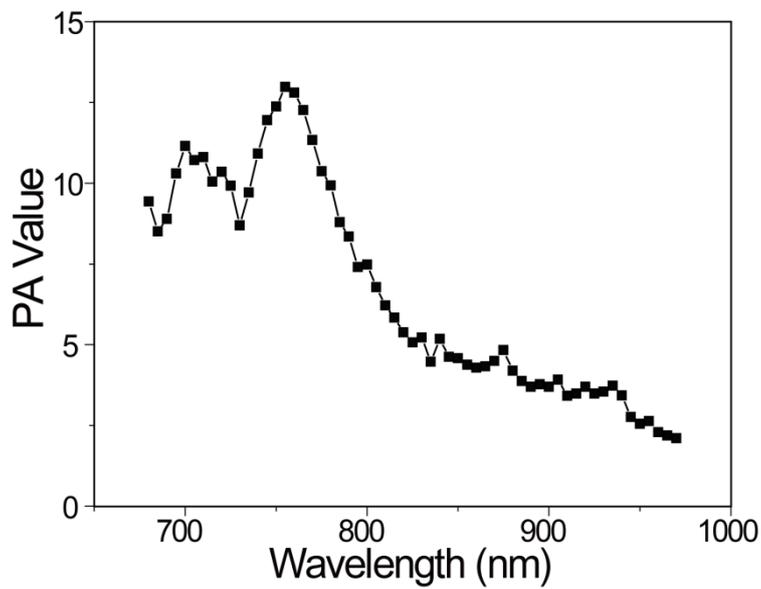
Figure S9. The photoacoustic signal amplitude of the nanoparticles between 680–970 nm *in vitro*. The peak signal occurs at 754 nm.
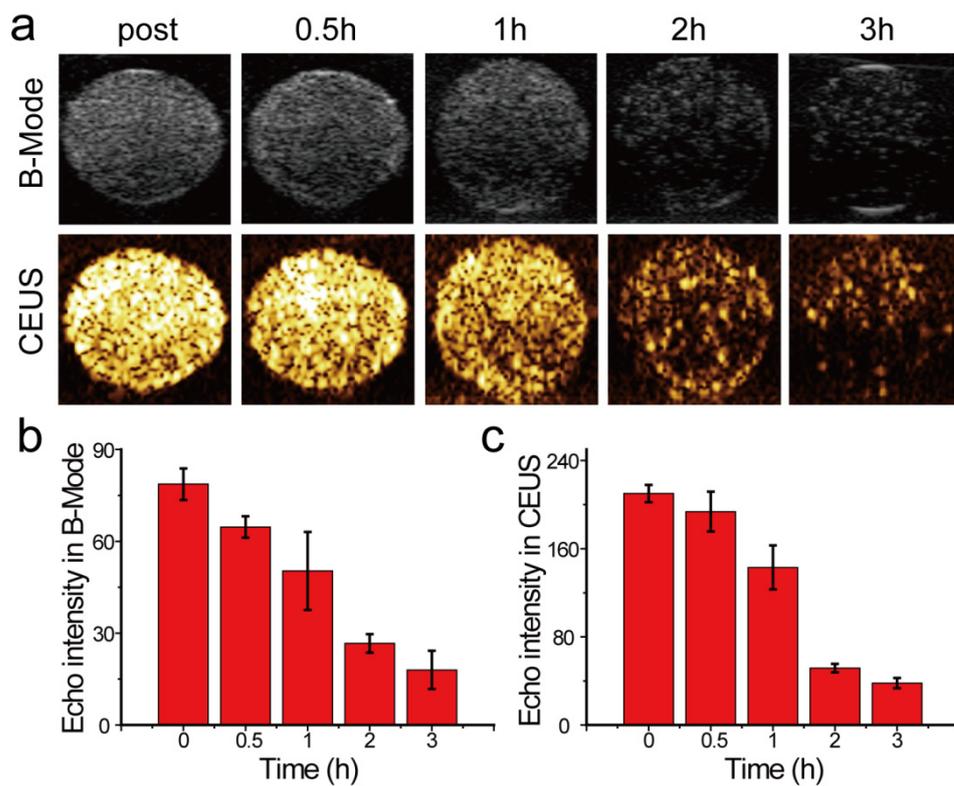
Figure S10. *In vitro* a) ultrasound imaging of the nanoparticles after laser irradiation, and the corresponding echo intensity in b) B-Mode and in c) CEUS up to 3 h post irradiation.
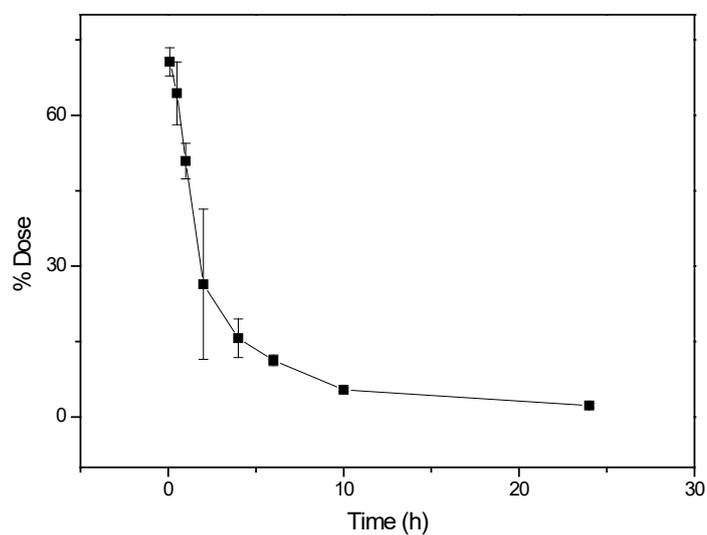
Figure S11. Blood clearance of the nanoparticles measured by a fluorescent spectrophotometer up to 24 h post-injection (mean ± SD, n = 3).
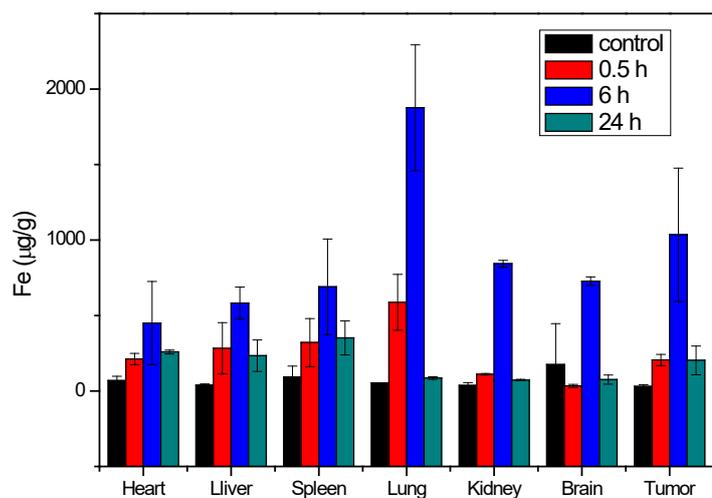
Figure S12. Time-dependent biodistribution of iron ion in the main organs and tumors (mean ± SD, n = 3).
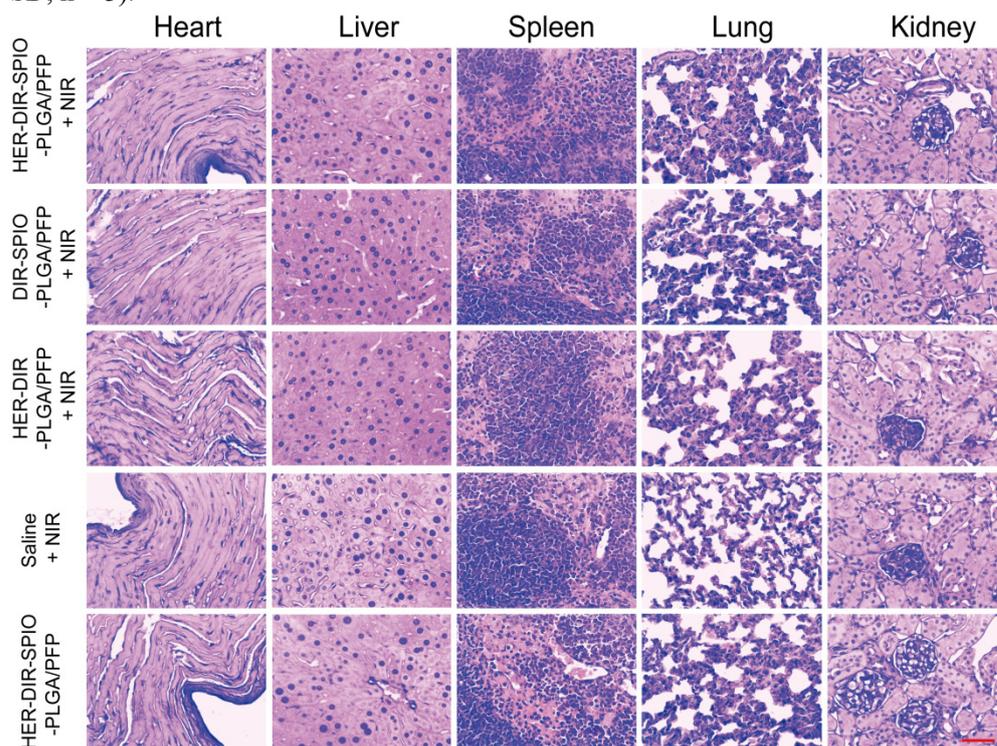
Figure S13. H&E stained tissue sections of major organs including the heart, liver, spleen, lung and kidney of mice 21 days after treatment with the HER2 targeted nanoparticles and the four controls. Magnification is 400×, scale bar is 100 μm.
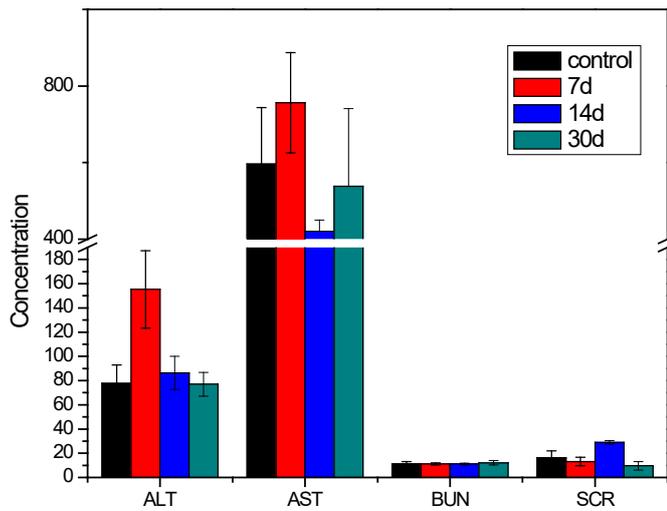
Figure S14. *In vivo* toxicology assessment. Blood biochemistry data including liver-function markers: ALT, AST, and kidney-function markers: BUN, SCR (mean ± SD, n = 4).
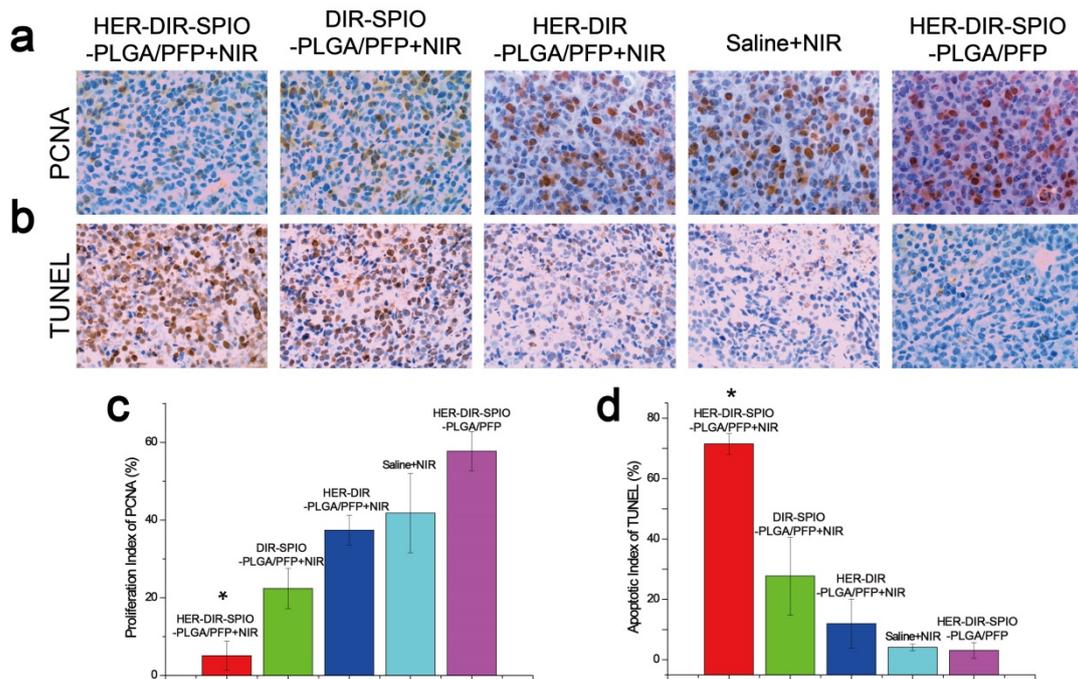
Figure S15. The expression of a) PCNA and b) TUNEL in tumor tissue by immunohistochemical staining. The nucleus appears brown for PCNA-positive or TUNEL-positive cells, and the blue represents the negative cells (400× magnification). c) The proliferation index (PI) of PCNA and d) apoptotic index (AI) of TUNEL in each group (*P < 0.05). These results show that the HER2 targeted nanoparticles had a significantly lower PI and higher AI than that of control groups.

Reference:

1. Roper DK, Ahn W, Hoepfner M. Microscale. Heat Transfer Transduced by Surface Plasmon

Resonant Gold Nanoparticles. J Phys Chem C Nanomater Interfaces. 2007; 111: 3636-41.